01

Modeling the thermal conductivity of black phosphorene using deep learning

© D.V. Zav'yalov,[1] D.N. Zharikov,[1] V.I. Konchenkov,[1,2]¶ D.V. Shein[1]

[1]Volgograd State Technical University,
400005 Volgograd, Russia
[2]Volgograd State Socio-Pedagogical University,
400005 Volgograd, Russia
¶e-mail: kontchenkov@yandex.ru

Received October 23, 2024
Revised October 23, 2024
Accepted October 23, 2024

With the help of a convolutional neural network with continuous filtering SchNet, trained on the simulation data by the Car-Parrinello quantum molecular dynamics method, the potential of the black phosphorene force field is constructed, applicable for use in the framework of modeling by the classical molecular dynamics method. The parameters of the neural network and the ways of its training are revealed, which allow us to build the most realistic representation of the force field. Using a force field calculated by a neural network, the thermal conductivity of a sample of black phosphorene in a LAMMPS package was simulated. The calculated values of thermal conductivity are consistent with the data obtained by other groups experimentally and within the framework of calculations.

Keywords: convolutional neural networks, the potential of interatomic interaction, classical molecular dynamics.

DOI: 10.61011/TP.2025.03.60846.358-24

Introduction

Black phosphorene, which has been discovered experimentally in 2014, is a two-dimensional material with a pronounced anisotropy of electronic and transport properties [1,2]. Black phosphorene is also of interest in the context of production of vertical heterostructures consisting of several layers of similar two-dimensional crystals (graphene, silicene, molybdenum sulfide, etc.) held together by van der Waals forces. Molecular dynamics simulation is a well-established method for study of van der Waals materials (see, e.g., [3–7]). Quantum molecular dynamics methods (of which the Born–Oppenheimer and Car-Parrinello methods are used most often [8]) provide physically sound models of atomic motion in the structures under consideration, but allow one to examine only modest-sized systems (containing several dozen atoms) on time scales on the order of hundreds of femtoseconds. Classical molecular dynamics methods provide an opportunity to calculate the motion of millions of particles on nanosecond time scales; the greatest challenge is to reproduce adequately the force field in a sample. An approach involving the use of neural networks for calculation of the interatomic interaction potential (force field), which is then used to calculate particle trajectories within classical molecular dynamics, has been progressing rapidly in recent times [3,9,10]. Since a training set is formed based on the results of *ab initio* molecular dynamics (AIMD) modeling of the studied molecules, this approach theoretically allows one to predict the force field with an accuracy typical of density functional theory methods.

Fully connected [11,12], graph [13–16], convolutional [17–19], and generative [20–21] neural networks are currently used widely in reconstruction of the interatomic interaction potential. The range of deep learning methods put to use is so wide due, first, to the need to test various types of material description and architectures and methods of training of neural networks in order to find those that represent the force field most accurately. Second, the structural features of the studied substances necessitate the application of a wide variety of networks, since networks of a certain type may characterize well the force field of certain materials, but are ill-suited for reproducing the interaction potential in other materials. Specifically, the applicability of a feed-forward neural network implemented in DeePMD [11] in calculations of the interatomic interaction potential of black phosphorene, which is a two-dimensional crystal, and polyphenylene sulfide, which is a polymer, was examined in [22]. It was found that the neural network used in [22] fails to account accurately for the specific features of the force field of polyphenylene sulfide, which is attributable to the fact that a polymer has a large (compared to a crystalline substance) number of configurations that need to be represented in the training set.

In the present study, an attempt is made to represent the force field in a sample using a neural network with an architecture different from DeePMD. We have chosen the SchNet network, which is a continuous-filter convolutional neural network and is included into the SchNetPack package [19]. This network is sometimes classified as a graph one (see, e.g., [16]), which is attributable to the specifics of representation of the list of neighbors of a chosen atom.

Just as in [22–24], black phosphorene is the sample under study. On the one hand, this material is fairly new, and the features of its electronic and phonon transport remain in the focus of attention of researchers. On the other hand, several studies concerned with the representation of the interatomic interaction potential in this material have already been published; therefore, the obtained results may be compared with the results reported by other research groups.

The actual comparison of the obtained force fields is just the first stage of assessment of the applicability of neural networks for modeling the material under consideration. One needs to calculate the value of a certain physical quantity and compare it with experimental data. The density and thermal conductivity of black phosphorene were calculated in [23,24] using a force field constructed by the neural network of the DeePMD package. The following values were obtained: armchair thermal conductivity $\kappa_{\text{armchair}} = 1.685\,\text{W/(m·K)}$, zigzag thermal conductivity $\kappa_{\text{zigzag}} = 2.552\,\text{W/(m·K)}$, and a density of $2.72\,\text{g/cm}^3$ (the experimental density value is $2.69\,\text{g/cm}^3$). It was assumed in calculations of the bulk density in [23,24] that the sample size in the direction perpendicular to the phosphorene plane is equal to distance $d \approx 5.455\,\text{Å}$ [25] between the layers of black phosphorus in the bulk sample. The test problem in the present study is the calculation of thermal conductivity of phosphorene, which allows for comparison with the results reported in [23,24]. In the future, it is planned to test the SchNet network in modeling of polymer materials. It is expected that, similar to how convolutional neural networks aggregate a large number of pixels in image processing, the SchNet continuous-filter convolutional neural network should allow one to take into account the configurational features of polymers that are beyond the reach of feed-forward networks. It should be noted that the majority of studies focused on SchNet involve the use of the QM9 and MD17 data sets (see references in [17]), which contain data for relatively small organic molecules. As far as we know, this network has not been used in studies of crystalline substances. The accuracy of calculation of force fields by neural networks of various types (SchNet included) was compared in [16]. Following [18], the authors of [16] prepared their own implementation of SchNet, which provided an opportunity to configure this network more precisely. An account of systematic errors in the representation of force fields by graph neural networks was presented in [16], and ways to reduce these errors were proposed.

The thermal conductivity of black phosphorus and, in particular, black phosphorene has been examined in several studies both theoretically and experimentally. The thermal stability of phosphorene in a graphene–phosphorene heterostructure was studied in [6] by the molecular dynamics method. It was demonstrated that a phosphorene sample enclosed between two graphene sheets acquires a significantly greater stability than free-standing phosphorene. The thermal conductivity of the material in such a heterostructure also increases significantly. The Stillinger–Weber potential [26] parameterized in [27] was used to model the interactions between phosphorus atoms in [6], and the Lennard-Jones potential was used to model the interaction between phosphorene and graphene sheets. The values of armchair thermal conductivity $\kappa_{\text{armchair}} = 2.5-4.5\,\text{W/(m·K)}$ and zigzag thermal conductivity $\kappa_{\text{zigzag}} = 10-22\,\text{W/(m·K)}$ of black phosphorene were obtained in [6]. The Stillinger–Weber potential was also used in [7,28–30] to model the properties of black phosphorene. Following [6], the authors of [29] have modeled a graphene–phosphorene heterostructure using the classical molecular dynamics method and calculated its thermal conductivity. The thermal stability of a heterostructure formed by a sheet of phosphorene and a phosphorus nanotube positioned on it was examined in [7]. The influence of boundaries on the electronic and phonon properties of phosphorene nanoribbons was investigated in [30]. Report [31] is focused on the first-principle study of thermal transport in black phosphorene; the methods of density functional theory were used to calculate the phonon dispersion, and the actual calculation of the thermal conductivity coefficient was based on the solution of the Boltzmann kinetic equation for phonons. The thermal conductivity values for black phosphorene given in [31] are as follows: $\kappa_{\text{armchair}} = 0.15-5.24\,\text{W/(m·K)}$ and $\kappa_{\text{zigzag}} = 0.51-30.48\,\text{W/(m·K)}$. This large spread in values is due to the fact that different models of pseudopotentials and exchange-correlation interaction functionals were used to optimize the structure and for subsequent calculations of the phonon spectrum by the density functional theory methods. The construction of an interatomic interaction potential for phosphorus in the form of a Gaussian approximation potential (GAP) [33], which relies on machine learning, was discussed in detail in [32]. Heat transfer processes in different modifications of phosphorene (black, blue, and violet) were studied in [34] via classical molecular dynamics modeling with the so-called neuroevolutional potential (NEP) [35]). The following values of the thermal conductivity coefficient were obtained for black phosphorene in [32]: $\kappa_{\text{armchair}} = 12.5\,\text{W/(m·K)}$ and $\kappa_{\text{zigzag}} = 78.4\,\text{W/(m·K)}$. The GPUMD package supporting the NEP potential was used in [34] to implement molecular dynamics; the accuracy and efficiency of these calculations was compared with the implementation of molecular dynamics in the LAMMPS package with the GAP potential. The thermal conductivity of thin-layer samples of black phosphorus was studied experimentally via Raman spectroscopy in [25]. A comparison of experimental data and various model approaches to the determination of thermal conductivity of black phosphorene was presented in [36].

The above literature data suggest that, first, the thermal conductivity of black phosphorene has a pronounced anisotropy and, second, the numerical values of thermal conductivity vary greatly between the studies performed by different research groups and depend on the modeling procedure. Two-dimensional phosphorus modifications

have a rather complex crystal structure, and their phonon spectra differ significantly from the spectra of bulk samples. Different estimates of the thermal conductivity coefficient are obtained when various aspects of phonon dynamics are taken into account (in modeling via density functional theory methods followed by solving the Boltzmann kinetic equation for phonons or in the case of selection of the interatomic interaction potential followed by modeling using the classical molecular dynamics method).

Generally speaking, the harmonic approximation for crystal lattice vibrations is expected to remain valid in calculations of the heat capacity and thermal conductivity of phosphorene at the considered temperatures (around 300 K), and the phonon–phonon interaction may be neglected. It is known from general physics that the lattice thermal conductivity in this case is given by

$$\kappa = \frac{1}{3} C u \langle \lambda \rangle, \qquad (1)$$

where C is the heat capacity of phonon gas per unit volume, u is the velocity of sound, and $\langle \lambda \rangle$ is the mean free path of phonons. The velocity of sound in phosphorene was determined several times (e.g., in [23]) based on the data from classical molecular dynamics simulations. In the harmonic approximation, when mechanisms leading to collisions between different phonons are neglected, the mean free path is specified exclusively by collisions of phonons with the boundary surfaces of a crystal and lattice defects. Further studies are needed to determine the conditions under which this approximation is applicable to a two-dimensional black phosphorene crystal. The mean free path may be determined indirectly based on the solution of the Boltzmann kinetic equation for phonons (see, e.g., [31]). At the same time, it was reported in several studies (see, e.g., [5]) that anharmonic interactions of the phosphorene lattice already manifest themselves at temperatures around 300 K. Modeling via the classical molecular dynamics method allows one to study the thermal conductivity of a sample without the preliminary introduction of model concepts of phonon dynamics and gain an insight into the crystal lattice vibrations based on statistical data. The accuracy of the obtained result depends strongly on the validity of the representation of the force field in the material. Therefore, the main objective of the present study is to evaluate the applicability of the potential calculated by the SchNet convolutional neural network in representing the interatomic interaction in a black phosphorene crystal in calculations of thermal conductivity.

1. SchNet simulation of the force field of black phosphorene

A fragment of the crystal lattice of black phosphorene, which is the material examined in the present study, is shown in Fig. 1, *a*. The training data were obtained by simulating a cell containing 16 atoms using the Car–Parrinello

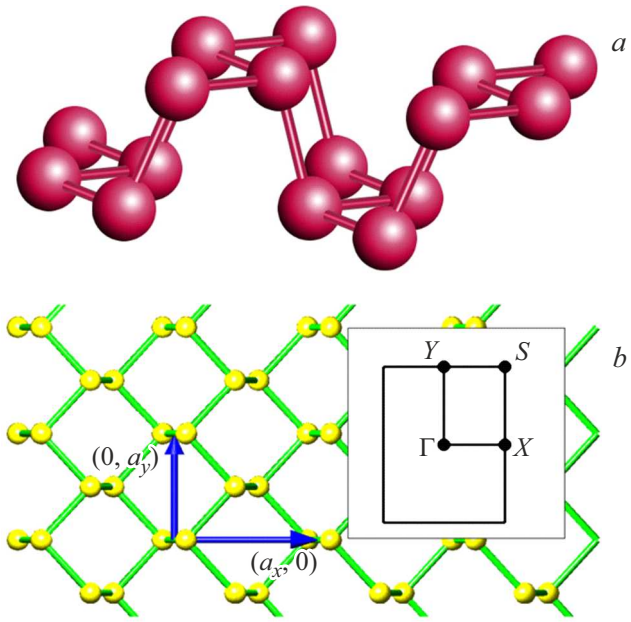

Figure 1. Crystal structure of black phosphorene: *a* — cell used for simulation; *b* — lattice translation vectors: $a_x = 4.376$ Å, $a_y = 3.314$ Å [1].

AIMD method implemented in the Quantum ESPRESSO package. The Nosé thermostat is used in modeling by the Car–Parrinello method. The thermostat oscillation frequency must be of the same order of magnitude as the phonon frequency (the specified frequency value was 100 THz). The thermostat temperature was 300 K. Two data sets containing 2000 and 10 0000 records were used for training. A record contains information about 16 atoms: the coordinates of each atom in three-dimensional space, three projections of the force acting on each atom, and the energy of the entire configuration of atoms.

The SchNetPack package includes the SchNet neural network itself, which is accessed either through the ASE-interface or via the command line. The ASE- interface is preferable, since it allows one to manage data, train a neural network, and use trained models within the Python code. The package also includes its own classical molecular dynamics module, which also based on ASE. This module was not used in the present study; classical molecular dynamics simulations were performed in the LAMMPS package. To do this, we had to build LAMMPS from source using plugins implementing „wrapper“ code to represent the LAMMPS force field style via a model file produced by training the SchNet neural network. This approach allows for a direct comparison of the performance of SchNet and DeePMD networks, since the difference in LAMMPS input files then comes down to replacing the reference to a file containing the model of the interatomic interaction potential generated by the trained neural network.

The architecture of the SchNet network is presented in Fig. 2. The molecule is represented atom-wise at each

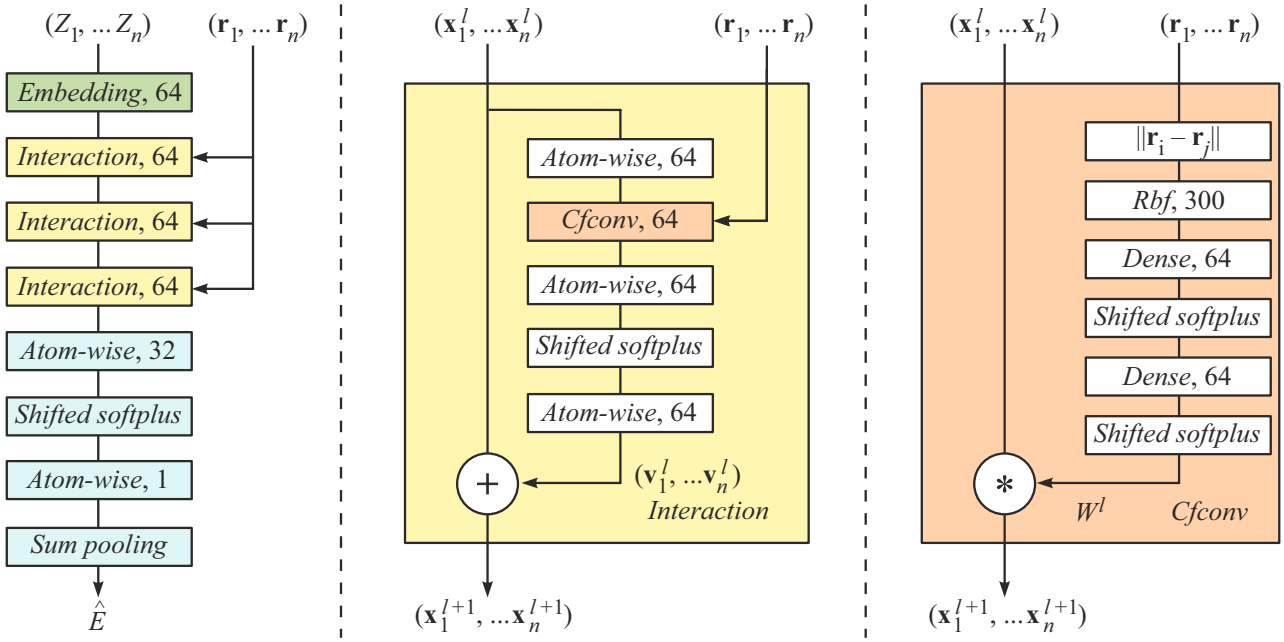

Figure 2. Architecture of SchNet [17].

layer of this network. Attribute vector $X_l = (x_1^l, x_2^l, \ldots, x_n^l)$ is formed from a combination of coordinates of all atoms $R = (\mathbf{r}_1, \mathbf{r}_2, \ldots, \mathbf{r}_n)$ and their charge numbers $Z = (Z_1, Z_2, \ldots, Z_n)$, n is the number of atoms in the molecule under study, and l is the order number of the neural network layer. Quantity x_i^l is a vector with length F, where F is specified by parameter n_atom_basis of class representation.SchNet.

At the initial stage ($l = 0$), attribute vectors x_i^0 are formed on the basis of embedding performed on the list of charge numbers. Information about the coordinates of atoms is then added to x_i^l in the interaction layers. These are the layers where convolution is performed. Tentatively speaking, an x_i^l set of F numbers stores information about the position of the i-th atom relative to the other atoms.

SchNetPack allows one to vary the following parameters:

— n_atom_basis (F) — number of feature map elements (eng. number of feature map);

— number of interaction layers (n_interactions), which is actually the number of convolutional layers;

— type of radial basis functions used and their number n_rbf (Fig. 2; rbf layer, cfconv block);

— cutoff radius, which sets the number of neighboring atoms taken into account;

— neighbor list construction algorithm.

Relying on the results of computational experiments and analysis of learning curves, we chose n_atom_basis = 256, n_interactions = 9, n_rbf = 300, cutoff = 5.0 Å, and the ASENeighborList algorithm for constructing a list of neighbors that allows one to introduce periodic boundary conditions. The type and number of radial basis functions were chosen as per the recommendations of the SchNet developers. The cutoff parameter value was chosen to be slightly larger than the lattice constant of black phosphorene ($a_x = 4.376$ Å, $a_y = 3.314$ Å [1]; Fig. 1, *b*). The specified neighbor list formation algorithm and the cutoff radius value impose restrictions on the batch size (batch_size parameter), which was set to 100−200 in calculations performed with the NVIDIA GeForce RTX 3060 video card (with larger batch_size values, video memory overflow was noted). The trained neural network receives the coordinates of atoms as input parameters; at the output, the values of force vectors acting on each atom and the total energy of the system are generated. Since a periodic structure is considered and it is planned to conduct subsequent modeling using the classical molecular dynamics method, the weighting coefficients for calculation of the loss function on the validation set were chosen to be 0.99 and 0.01 for forces and energies, respectively. The mean-square error is used as the loss function.

Figure 3 shows the val_loss (loss function on the validation set) plots for two network training options: *1* — data set DS1 with 2000 records, the training, validation, and test set sizes are num_train = 1200, num_val = 600, and num_test = 200, respectively, and periodic boundary conditions are not introduced; *2* — data set DS2 with 10 0000 records, num_train = 80 000, num_val = 15 000, num_test = 5000, and periodic boundary conditions at the boundaries of the crystal region shown in Fig. 1, *a* are taken into account.

It is evident from Fig. 3 that the loss function reaches a plateau in both cases; as expected, the steady-state val_loss value for a larger set with periodic boundary conditions introduced is lower.

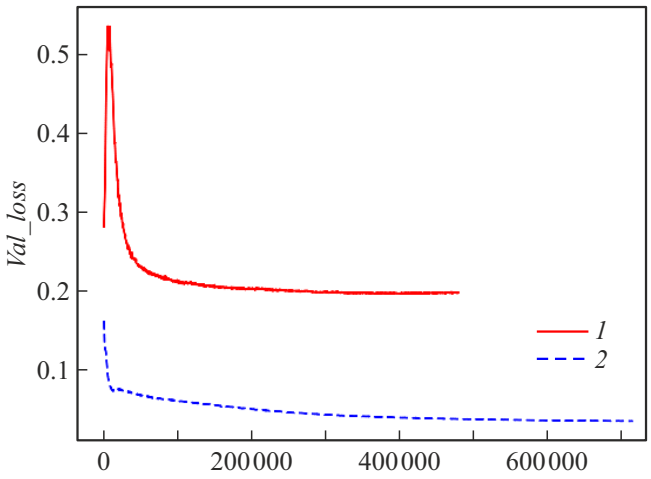

Figure 3. Loss function on the validation set: *1* — data set DS1 (2000 records); *2* — data set DS2 (100 000 records). The horizontal axis shows the number of neural network training iterations.

Histograms (Figs. 4, 5) of the distribution of absolute values of force acting on each phosphorus atom in the unit simulation cell (Fig. 1) allow one to compare the quality of prediction of force fields. Figure 6 presents the distribution of absolute values of forces acting on a phosphorus atom obtained by combining data on the distribution of moduli of forces acting on each of the atoms shown in Figs. 4, 5. The absolute values of force in units of eV/Åare plotted on the horizontal axis in Figs. 4–6, and the vertical axis shows the number of such values falling within the given $(F, F + \Delta F)$ interval. The presented dependencies are normalized in such a way that the area under the curve of distribution of the moduli of forces acting on a phosphorus atom is equal to unity. In Figs. 4, 5, the histograms of the distribution of force moduli corresponding to the initial AIMD-based data and the data generated by both force field models agree well for a fraction of atoms, while the distributions of force moduli provided by the neural network models for the remaining atoms are shifted downward. It follows from Fig. 6 that, on average, both models provide a somewhat underestimated absolute force value. It should be noted that when a phosphorene sample is brought to thermodynamic equilibrium in molecular dynamics, the best results are provided by the model trained on the smaller DS1 data set. It has already been reported (see, e.g., [37]) that the SchNet network trained on sets of several thousand records yields more accurate results than the one trained on hundreds of thousands of records. In Fig. 6, the distribution of absolute values of forces acting on an atom obtained via machine learning with a set of 100 000 records is closer to the distribution derived from the initial AIMD- simulation data (compared to the distribution of absolute values of forces obtained with a set of 2000 records).

2. Thermal conductivity modeling

The method for calculating thermal conductivity detailed in the LAMMPS package manual (fix heat command) was used. A sample obtained by replicating the crystal region shown in Fig. 1, *a* 23 times along the X axis (along the armchair boundary) and 16 times along the Y axis (along the zigzag boundary) was examined in calculations of the armchair thermal conductivity. The total number of phosphorus atoms was 5888. The length of the sample along the X axis was $l_x = 202.5$ Å; its length along axis Y $l_y = 105.3$ Å (Fig. 7). The width of the heat source and sink region was $\Delta l = 10$ Å. Since periodic boundary conditions were used, we positioned the heat source and the heat sink at the edge and at the center of the sample, respectively. In a similar fashion, the zigzag thermal conductivity was calculated for a sample obtained by replicating the crystal region shown in Fig. 1, *a* 12 times along the X axis and 31 times along the Y axis. In this case, $l_x = 105.7$ Å, $l_y = 204$ Å, and the total number of atoms was 5952.

Thermal conductivity coefficient κ is defined as the coefficient of proportionality between heat flux J and the temperature gradient: ∇T:

$$\mathbf{J} = -\kappa \nabla T. \tag{2}$$

In the configuration presented in Fig. 7, the thermal energy flux along the X axis is considered; therefore expression (2) is reduced to the one-dimensional case:

$$J = -\kappa(\nabla T)_x = -\kappa \frac{dT}{dx} \approx -\kappa \cdot \Delta T / \left(\frac{l_x}{2}\right), \tag{3}$$

where ΔT is the temperature difference between the heat source and the heat sink and $l_x/2$ is the distance between them.

Heat flux is defined as the amount of heat passing through the sample cross section per unit time:

$$J = \frac{\Delta Q}{\Delta t \cdot S}. \tag{4}$$

Combining (3) and (4), we obtain

$$\kappa = \frac{\Delta Q}{\Delta t \cdot S} \frac{l_x}{2} \frac{1}{\Delta T}. \tag{5}$$

Thermal conductivity values are calculated in LAMMPS based on time averaging of the temperature difference between the heat source and the heat sink.

Since the studied sample is two-dimensional, we take distance $d \approx 5.455$ Åbetween the phosphorene layers [25] in a bulk sample as the dimension along the Z axis, so that $S = d \cdot l_y$. Thus, the armchair thermal conductivity of the black phosphorene sample is given by

$$\kappa_{\text{armchair}} = \kappa_x = \frac{\Delta Q}{\Delta t \cdot l_y \cdot d} \frac{l_x}{2} \frac{1}{\Delta T}, \tag{6}$$

and its zigzag thermal conductivity is written as

$$\kappa_{\text{zigzag}} = \kappa_y = \frac{\Delta Q}{\Delta t \cdot l_x \cdot d} \frac{l_y}{2} \frac{1}{\Delta T}. \tag{7}$$

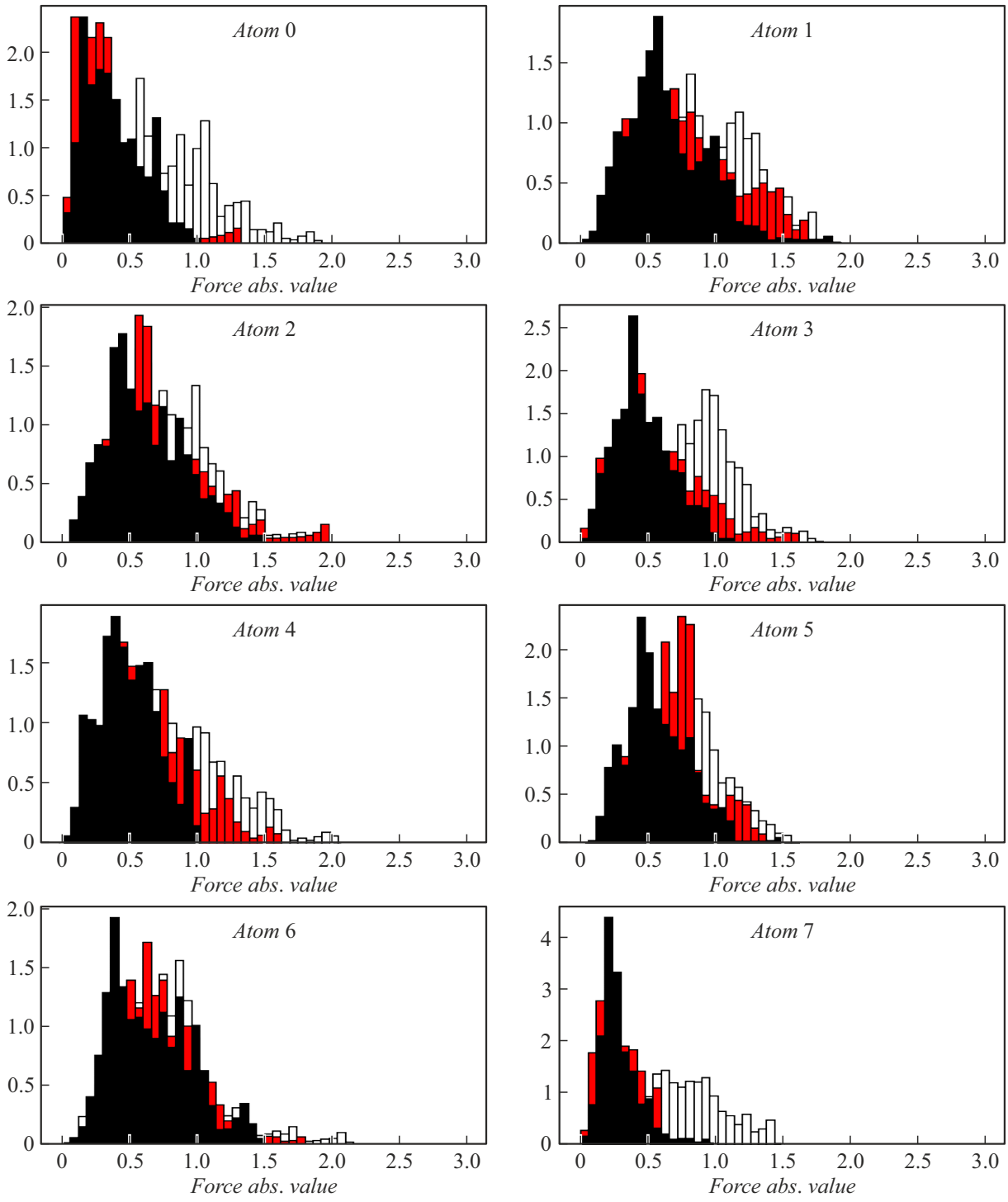

Figure 4. Comparison of histograms of the distribution of absolute values of forces acting on an atom for each of the model atoms (atoms 0–7). White histogram — AIMD data; black histogram — force field calculated by the network trained on data set DS1; red histogram — force field calculated by the network trained on DS2.

The simulation of thermal conductivity in LAMMPS is carried out in two stages. At the first stage, the system is brought to equilibrium at a temperature of 273 K: 10 000 steps in „heating“ from 0 to 20 K using the NVE ensemble and the Berendsen thermostat with rate adjustments at each time step; 20 000 steps in heating from 20 to 273 K using the NVE ensemble and the Berendsen thermostat with rate adjustments every 100 steps; and 10 000 steps with the temperature maintained at 273 K using the NVT ensemble with rate adjustments every 100 steps. One time step corresponds to 1 fs. At the second stage, we set the position of the „hot“ and „cold“ blocks (heat source and

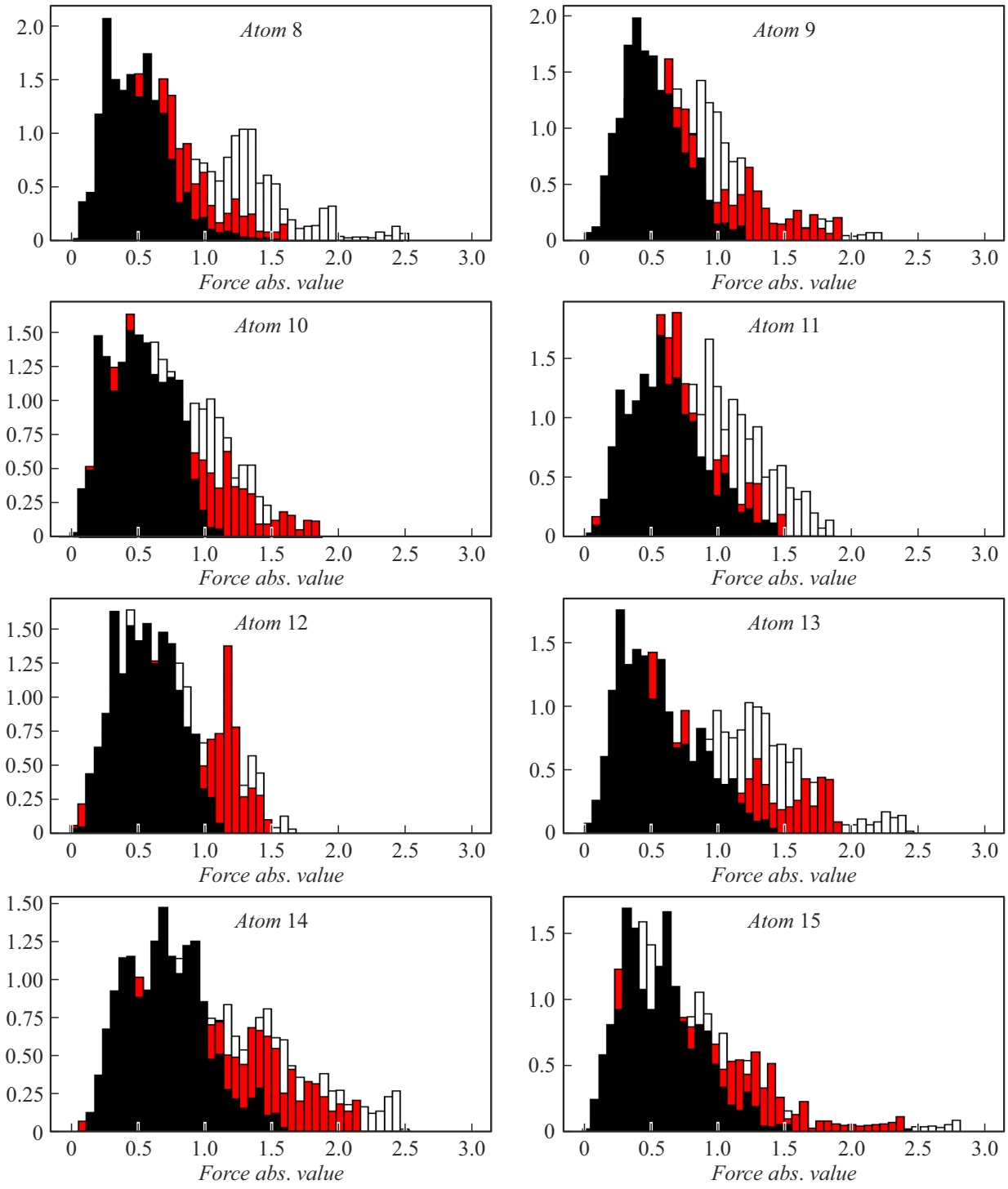

Figure 5. Comparison of histograms of the distribution of absolute values of forces acting on an atom for each of the model atoms (atoms 8–15). White histogram — AIMD data; black histogram — force field calculated by the network trained on data set DS1; red histogram — force field calculated by the network trained on DS2.

sink), use the NVT ensemble with rate adjustments every 100 steps (10 000 steps in total), and calculate the average temperature difference between the blocks. Averaging is performed every 200 time steps, the initial data are updated every 20 steps, and 6 previous values corresponding to the moments of updating the initial data are used in averaging.

The thermal conductivity values obtained in modeling of heat transmission along the armchair and zigzag boundaries are $\kappa_{\text{armchair}} \approx 3\,\text{W/(m·K)}$ and $\kappa_{\text{zigzag}} \approx 11\,\text{W/(m·K)}$. On the one hand, thermal conductivity has a pronounced anisotropy, which has already been reported in a number of experimental and theoretical studies of black phosphorene.

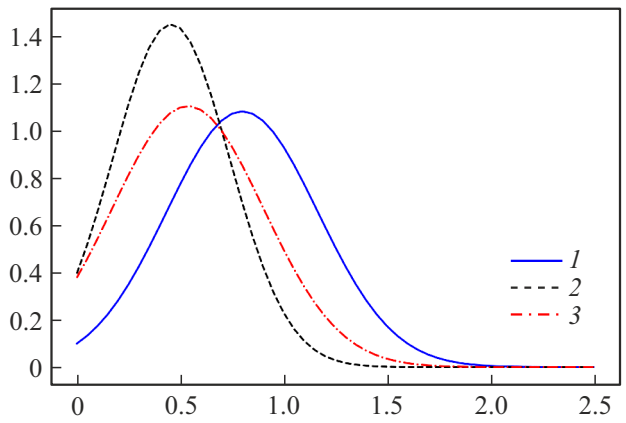

Figure 6. Comparison of distributions of absolute values of forces acting on an atom for all atoms of the model. Blue solid curve *1* — AIMD data; black dotted cure *2* — force field calculated by the network trained on data set DS1; red dash-and-dot curve *3* — force field calculated by the network trained on DS2.

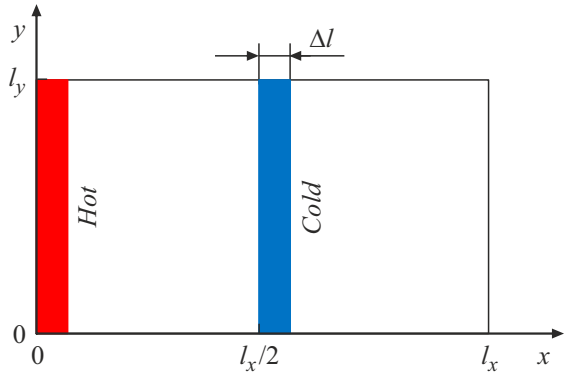

Figure 7. The positioning of the heat source (Hot) and sink (Cold) regions in modeling of the thermal conductivity of the sample along the *X* axis.

On the other hand, the values obtained earlier in [23,24] are several times smaller. This is likely attributable to the lower accuracy of the interatomic interaction potential generated by the SchNet network (compared to the potential generated by DeePMD).

3. Discussion

It can be seen from Figs. 4–6 that although the potential model presented by the neural network does, on average, underestimate the magnitudes of forces acting on atoms in both cases, the results provided by the model trained on a set containing 2000 records are largely similar to those of the model trained on a set containing 100 000 records. This is likely attributable to the specifics of implementation of the SchNetPack package. The calculations are organized in such a way that the learning rate changes only after a full epoch has passed (when all values from the training set have been fed to the input of the neural network). Being a crystalline substance, black phosphorene features a small (compared to amorphous materials) number of different configurations that need to be taken into account. The network is trained by gradient descent, and the learning rate, which determines the step size in moving toward the minimum of the loss function, should preferably be recalculated as soon as the introduction of new data ceases to alter significantly the loss function value. If the loss function barely changes after the neural network has been presented with the first few thousand records, while the learning rate is recalculated only after the neural network has been presented with several tens of thousands of records, a significant amount of unnecessary computational work, which does not lead to any significant enhancement of accuracy of the prediction of the force field by the generated model, is performed. The issue of accuracy of prediction of the interatomic interaction potential by graph neural networks, of which SchNet is an example, was examined systematically in [16]. Among other methods for reducing the force field prediction errors, the authors of [16] propose the use of ensembles of neural networks with different architectures or different settings trained on the same data with subsequent averaging of the obtained predictions in a certain way. Another option would be to train a neural network on different subsets from the training set and process the results in a similar way to how multiple trees are used in the random forest algorithm.

The calculated thermal conductivity values of black phosphorene correlate with the results reported by other research groups. However, the DeePMD network is more accurate in selecting the interatomic interaction potential for black phosphorene than SchNet. The developers of SchNetPack have recently expanded the package by adding the FieldSchNet, PaiNN, and SO3net [19] networks, which are built on slightly different principles than SchNet. Preliminary studies, where the problem of equilibrating a phosphorene sample was used an example, performed using the classical molecular dynamics module of the SchNetPack package with a potential calculated by the PaiNN network revealed that the sample remains stable, long-range ordering is preserved, and the amplitude of temperature fluctuations is significantly smaller than the one obtained with a potential calculated by the SchNet network. In addition, the simplest method for calculating thermal conductivity provided by the LAMMPS package was used in the present study. The use of other methods should make it possible to obtain a more accurate value of thermal conductivity of phosphorene.

Conclusion

The SchNet network was configured and trained to obtain the interatomic interaction potential of black phosphorene, and a comparison of histograms of the distribution of magnitudes of forces acting on an atom corresponding to different data sets and training methods was performed. The molecular dynamics method implemented in the LAMMPS

package was used to bring the system to equilibrium, and the thermal conductivity of a sample along the „armchair“ and „zigzag“ boundaries was calculated. Compared to the data obtained with the potential calculated by the DeePMD package, the approach used in the present study yields overestimated values of thermal conductivity in both directions. The main result is that the SchNet network, which has previously been used mostly for modeling the energy and forces of interatomic interactions of small organic molecules, was found to be applicable in modeling of the force field of black phosphorene (a two-dimensional crystalline material), although the accuracy of the resulting model is lower than that of the model provided by the DeePMD network.

Acknowledgments

The computational cluster of the Volgograd State Technical University (VSTU) was used in this study. The authors wish to thank A.E. Andreev, the head of the Department of Electronic Computers and Systems (VSTU), and D.L. Abdrakhmanov, a lecturer at the Department of Electronic Computers and Systems (VSTU), for their assistance in setting up computing packages on the cluster.

Funding

This study was supported by grant No. 23-22-00461 from the Russian Science Foundation „Study of the thermal properties of ordered and disordered low-dimensional materials by molecular simulation with potentials obtained using deep machine learning“ (2022 tender „Fundamental and exploratory scientific research conducted by small-scale separate research teams“).

Conflict of interest

The authors declare that they have no conflict of interest.

References

[1] P. Li, I. Appelbaum. Phys. Rev. B, **90**, 115439 (2014). DOI: 10.1103/PhysRevB.90.115439
[2] M. Galluzzi, Y. Zhang, X.-F. Yu. J. Appl. Phys., **128**, 230903 (2020). DOI: 10.1063/5.0034893
[3] Zh. Fan, Y. Xiao, Y. Wang, P. Ying, Sh. Chen, H. Dong. J. Phys.: Condens. Matter, **36** (24), 245901 (2024). DOI: 10.1088/1361-648X/ad31c2
[4] K.A. Krylova, L.R. Safina, R.T. Murzaev, S.A. Shcherbinin, Yu.A. Baimova, R.R. Mulyukov. Phys. Solid State, **65** (9), 1514 (2023). DOI: 10.21883/FTT.2023.09.56256.101
[5] P. Anees. J. Phys.: Condens. Matter, **32** (33), 335402 (2020). DOI: 10.1088/1361-648X/ab8761
[6] Q.-X. Pei, X. Zhang, Zh. Ding, Y.-Y. Zhang, Y.-W. Zhang. Phys. Chem. Chem. Phys., **19**, 17180 (2017). DOI: 10.1039/C7CP02553J
[7] J. Wu, S. Chen, Ch. Chen, Y. Ma, Y. Tian. arXiv:2010.11414 (2020). DOI: 10.48550/arXiv.2010.11414
[8] M.E. Tuckerman. J. Phys.: Condens. Matter, **14**, R1297 (2002). DOI: 10.1088/0953-8984/14/50/202
[9] J. Han, L. Zhang, R. Car, W. E. Commun. Comput. Phys., **23** (3), 629 (2018). DOI: 10.4208/cicp.OA-2017-0213
[10] L. Zhang, J. Han, H. Wang, R. Car, W. E. Phys. Rev. Lett., **120**, 143001 (2018). DOI: 10.1103/PhysRevLett.120.143001
[11] J. Zeng, D. Zhang, D. Lu, P. Mo, Z. Li, Y. Chen, M. Rynik, L. Huang, Z. Li, Sh. Shi, Y. Wang, H. Ye, P. Tuo, J. Yang, Y. Ding, Y. Li, D. Tisi, Q. Zeng, H. Bao, Y. Xia, J. Huang, K. Muraoka, Y. Wang, J. Chang, F. Yuan, S.L. Bore, Ch. Cai, Y. Lin, B. Wang, J. Xu, J.-X. Zhu, Ch. Luo, Y. Zhang, R.E.A. Goodall, W. Liang, A.K. Singh, S. Yao, J. Zhang, R. Wentzcovitch, J. Han, J. Liu, W. Jia, D.M. York, W.E.R. Car, L. Zhang, H. Wang. J. Chem. Phys., **159** (5), 054801 (2023). DOI: 10.1063/5.0155600
[12] D. Lu, H. Wang, M. Chen, L. Lin, R. Car, W. E, W. Jia, L. Zhang. Comput. Phys. Commun., **259**, 107624 (2021). DOI: 10.1016/j.cpc.2020.107624
[13] I. Batatia, Ph. Benner, Y. Chiang, A.M. Elena, D.P. Kovács, J. Riebesell, X.R. Advincula, M. Asta, M. Avaylon, W.J. Baldwin, F. Berger, N. Bernstein, A. Bhowmik, S.M. Blau, V. Cărare, J.P. Darby, S. De, F.D. Pia, V.L. Deringer, R. Elijošius, Z. El-Machachi, F. Falcioni, E. Fako, A.C. Ferrari, A. Genreith-Schriever, J. George, R.E.A. Goodall, C.P. Grey, P. Grigorev, Sh. Han, W. Handley, H.H. Heenen, K. Hermansson, C. Holm, J. Jaafar, S. Hofmann, K.S. Jakob, H. Jung, V. Kapil, A.D. Kaplan, N. Karimitari, J.R. Kermode, N. Kroupa, J. Kullgren, M.C. Kuner, D. Kuryla, G. Liepuoniute, J.T. Margraf, I.-B. Magdău, A. Michaelides, J. Harry Moore, A.A. Naik, S.P. Niblett, S.W. Norwood, N. O'Neill, C. Ortner, K.A. Persson, K. Reuter, A.S. Rosen, L.L. Schaaf, C. Schran, B.X. Shi, E. Sivonxay, T.K. Stenczel, V. Svahn, C. Sutton, T.D. Swinburne, J. Tilly, C. van der Oord, E. Varga-Umbrich, T. Vegge, M. Vondrák, Y. Wang, W.C. Witt, F. Zills, G. Csányi. arXiv:2401.00096 (2024). DOI: 10.48550/arXiv.2401.00096
[14] B. Deng, P. Zhong, K. Jun, J. Riebesell, K. Han, C.J. Bartel, G. Ceder. Nat. Mach. Intell., **5**, 1031 (2023). DOI: 10.1038/s42256-023-00716-3
[15] C. Chen, S.P. Ong. Nature Comput. Sci., **2**, 748 (2022). DOI: 10.1038/s43588-022-00349-3
[16] T. Wollschläger, N. Gao, B. Charpentier, M.A. Ketata, S. Günnemann. ICML'23: *Proceedings of the 40th International Conference on Machine Learning* (Honolulu, Hawaii, USA, 2023), Art. № 1547, p. 37133–37156 (2023). https://dl.acm.org/doi/10.5555/3618408.3619955 [arXiv:2306.14916 (2023). DOI: 10.48550/arXiv.2306.14916]
[17] K.T. Schütt, H.E. Sauceda, P.-J. Kindermans, A. Tkatchenko, K.-R. Müller. J. Chem. Phys., **148**, 241722 (2018). DOI: 10.1063/1.5019779
[18] K.T. Schütt, P. Kessel, M. Gastegger, K.A. Nicoli, A. Tkatchenko, K.-R. Müller. J. Chem. Theory Comput., **15** (1), 448 (2019). DOI: 10.1021/acs.jctc.8b00908
[19] K.T. Schütt, S.S.P. Hessmann, N.W.A. Gebauer, J. Lederer, M. Gastegger. J. Chem. Phys., **158** (14), 144801 (2023). DOI: 10.1063/5.0138367
[20] N.W.A. Gebauer, M. Gastegger, K.T. Schütt. Adv. Neural Information Process. Systems, **32** (2019). https://proceedings.neurips.cc/paper_files/paper/2019/file/a4d8e2a7e0d0c102339f97716d2fdfb6-Paper.pdf [arXiv.1906.00957 (2020). DOI: 10.48550/arXiv.1906.00957]

[21] N.W.A. Gebauer, M. Gastegger, S.S.P. Hessmann, K.-R. Müller, K.T. Schütt. Nat. Commun., **13**, 973 (2022). DOI: 10.1038/s41467-022-28526-y
[22] D.V. Shein, D.V. Zav'yalov, V.I. Konchenkov. Zh. Tekh. Fiz., **93** (12), 1732 (2023). DOI: 10.61011/JTF.2023.12.56806.f242-23
[23] D. Shein, D. Zav'yalov. Eur. Phys. J. Plus, **139**, 863 (2024). DOI: 10.1140/epjp/s13360-024-05685-z
[24] D.V. Shein, D.V. Zav'yalov, D.N. Zharikov. Tezisy dokladov IX Mezhdunarodnoi molodezhnoi nauchnoi konferentsii „Fizika. Tekhnologii. Innovatsii“ (Ekaterinburg, 2022), p. 330 (in Russian).
[25] Zh. Luo, J. Maassen, Y. Deng, Y. Du, R.P. Garrelts, M.S. Lundstrom, P.D. Ye, X. Xu. Nat. Commun., **6**, 8572 (2015). DOI: 10.1038/ncomms9572
[26] F.H. Stillinger, T.A. Weber. Phys. Rev. B, **31**, 5262 (1985). DOI: 10.1103/physrevb.31.5262
[27] J.-W. Jiang. Nanotechnology, **26**, 315706 (2015). DOI: 10.1088/0957-4484/26/31/315706
[28] J.-W. Jiang, T. Rabczuk, H.S. Park. Nanoscale, **7**, 6059 (2015). DOI: 10.1039/c4nr07341j
[29] T. Liang, P. Zhang, P. Yuan, S. Zhai. Phys. Chem. Chem. Phys., **20**, 21151 (2018). DOI: 10.1039/C8CP02831A
[30] S.-Q. LI, X. Liu, X. Wang, H. Liu, G. Zhang, J. Zhao, J. Gao. Small, **18**, 2105130 (2022). DOI: 10.1002/smll.202105130
[31] F. Zhang, X. Zheng, H. Wang, L. Ding, G. Qin. Mater. Adv., **3**, 5108 (2022). DOI: 10.1039/D2MA00407K
[32] V.L. Deringer, M.A. Caro, G. Csanyi. Nat. Commun., **11**, 5461 (2020). DOI: 10.1038/s41467-020-19168-z
[33] A.P. Bartok, M.C. Payne, R. Kondor, G. Csanyi. Phys. Rev. Lett., **104**, 136403 (2010). DOI: 10.1103/PhysRevLett.104.136403
[34] P. Ying, T. Liang, K. Xu, J. Xu, Zh. Fan, T. Ala-Nissila, Zh. Zhong. Int. J. Heat Mass Transf., **202**, 123681 (2023). DOI: 10.1016/j.ijheatmasstransfer.2022.123681
[35] Z. Fan, Z. Zeng, C. Zhang, Y. Wang, K. Song, H. Dong, Y. Chen, T. Ala-Nissila. Phys. Rev. B, **104**, 104309 (2021). DOI: 10.1103/PhysRevB.104.104309
[36] G. Qin, X. Zhang, Sh.-Y. Yue, Zh. Qin, H. Wang, Y. Han, M. Hu. Phys. Rev. B., **94**, 165445 (2016). DOI: 10.1103/PhysRevB.94.165445
[37] K. Khrabrov, I. Shenbin, A. Ryabov, A. Tsypin, A. Telepov, A. Alekseev, A. Grishin, P. Strashnov, P. Zhilyaev, S. Nikolenko, A. Kadurin. Phys. Chem. Chem. Phys., **24**, 25853 (2022). DOI: 10.1039/d2cp03966d

Translated by D.Safin